Experimental decision on the electromagnetic momentum expression for magnetic media

1982 J. Phys. A: Math. Gen. 15 303

(http://iopscience.iop.org/0305-4470/15/1/038)

J. Phys. A: Math. Gen. **15** (1982) 303–318. Printed in Great Britain

Experimental decision on the electromagnetic momentum expression for magnetic media

D G Lahoz and G M Graham

Department of Physics, University of Toronto, Toronto, Ontario, Canada M5S 1A7

Received 24 April 1981, in final form 2 July 1981

Abstract. An experiment is described which discriminates between the two serious candidates for the correct expression of the electromagnetic momentum density within magnetic media, namely, $(1/c^2)\boldsymbol{E}\times\boldsymbol{H}$ and $\varepsilon_0\boldsymbol{E}\times\boldsymbol{B}$. The corresponding predictions of both theories regarding the torques arising on the parts of a capacitor with magnetic material as dielectric are thoroughly examined. Final measurements are reported using three different magnetic samples (ferrites) at ~4.2 K. The results conclusively expose the inadequacy of the $(1/c^2)\boldsymbol{E}\times\boldsymbol{H}$ theory and vindicate, within the experimental errors, the Livens proposal, $\varepsilon_0\boldsymbol{E}\times\boldsymbol{B}$. A short concluding remark is presented on the linear mechanical momentum balance when uniform Poynting vector is present within a permanent magnet.

1. Introduction

This work reports the final results of an experiment which allows a decision on whether the electromagnetic momentum density within magnetic matter is adequately expressed as $(1/c^2)\boldsymbol{E}\times\boldsymbol{H}$ or rather by $\varepsilon_0\boldsymbol{E}\times\boldsymbol{B}$. The first alternative (orthodox, say) has been accepted by a vast majority of authors (Einstein and Laub 1908, Landau and Lifshitz 1960, Penfield and Haus 1967, Novak 1980) whereas the second, proposed by Livens (1918), has had few supporters in the past (Page and Adams 1940). Recently Lahoz and Graham (1981) have presented a theoretical discussion of the problem, concluding that the Livens expression $\varepsilon_0\boldsymbol{E}\times\boldsymbol{B}$ is in fact more consistent with the currently accepted model for a magnetic dipole (spining electron) as a current loop. This conclusion was also in agreement with preliminary results (Lahoz and Graham 1979b) and further data (§ 5) which motivated our theoretical revision.

Schematically the experiment consists (figure 1) of the measurement of an alternating torque which appears on a material system S which is mechanically rigid and in exclusive interaction with the electromagnetic angular momentum localised in a vacuum cylindrical shell V. This volume V is also occupied by a magnetic material acting as the dielectric of a cylindrical capacitor which, together with its radial leads R, consistutes the system S. The axial $\mu_0\boldsymbol{H}$ field is produced by a superconducting coil C which does not exchange angular momentum with S, since its currents are azimuthal. Introductorily we can assume that the $\boldsymbol{E}$ field is only present within the shell V (magnetic sample) and that the small forces on the elastic fibres F do not exchange torques with S due to their proximity to the axis. Consequently when a low-frequency

0305-4470/82/010303+16$02.00

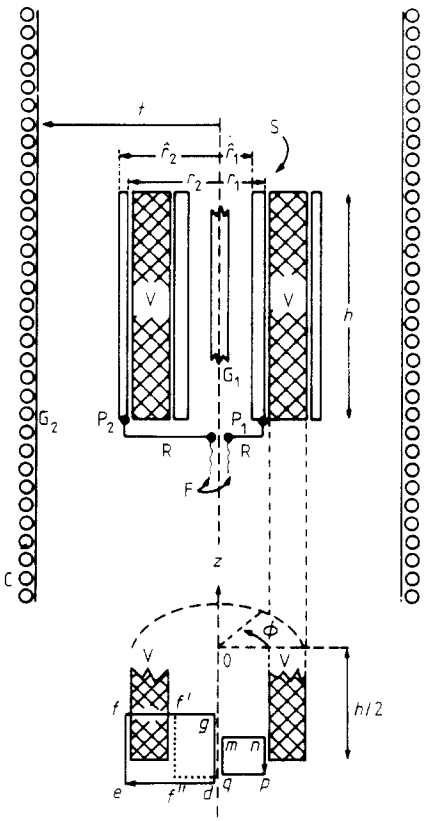

Figure 1. Schematic diagram (not to scale) of the capacitor and its radial leads.

voltage is applied to F a measurable torque on S appears given by

$$\boldsymbol{T}_{\text{orth}} = -\int_{\text{V}} \boldsymbol{r} \times \left(\frac{1}{c^2} \frac{\partial}{\partial t} (\boldsymbol{E} \times \boldsymbol{H}) \right) \text{dV} \tag{1}$$

or

$$\boldsymbol{T}_{\text{Livens}} = -\int_{\text{V}} \boldsymbol{r} \times \left(\varepsilon_0 \frac{\partial}{\partial t} (\boldsymbol{E} \times \boldsymbol{B}) \right) \text{dV} \tag{2}$$

according to the theories in question. These and no others (Lahoz and Graham 1981) could be considered as phenomenologically adequate in the low-frequency range; however the results to be presented here conclusively rule out (1) and are consistent with (2). Essential for such a crucial decision has been the use of a magnetic material with large remanence (barium-ferrite), along with other improvements added to our preliminary work (Lahoz and Graham 1979b).

2. Theory of the experiment

If in the oversimplified scheme presented in the Introduction the cylindrical capacitor had no other dielectric but vacuum (Graham and Lahoz 1980, 1981), the torque

amplitude acting on the system S would be entirely due to Lorentz force on the radial conduction current at R which is returned as vacuum displacement current through the capacitor, $C_{vac}\omega V_0$, where C_{vac} is the capacitance and V_0 is the voltage amplitude at frequency $\omega/2\pi$ across the cylindrical plates. Thus

$$T_0^{calc} \simeq \int_{r_1}^{r_2} rC_{vac}\omega V_0\mu_0 H_{ext}\,dr = \frac{V_0\omega}{2}(r_2^2-r_1^2)C_{vac}\mu_0 H_{ext}. \tag{3}$$

In this limiting case (3) is clearly equivalent to either (1) or (2) (compare the transition from formula (11) to (12) in Lahoz and Graham (1979a)). In the actual experiment it requires a correction because G_2 and G_1 (figure 1) were grounded and, analysing the system at $t=t_0$ such that the potentials of P_2 and P_1 are $+V$ ($\dot{V}>0$) and $-V$ respectively, the torque amplitude (3) due to $\mu_0 H_{ext}$ will be incremented by Lorentz forces on radial currents in R which leak to G_2 and G_1 through respective vacuum capacitances C_2 (electrodes P_2 and G_2) and C_1 (electrodes P_1 and G_1). Therefore the actual torque amplitude due to $\mu_0 \boldsymbol{H}_{ext}$ (essentially parallel to the $0z$ axis) is

$$T_0^{calc(\mu_0 H_{ext})} = \tfrac{1}{2}\mu_0 H_{ext} V_0\omega[(r_2^2-r_1^2)C_{vac}+\tfrac{1}{2}C_2\hat{r}_2^2-\tfrac{1}{2}C_1\hat{r}_1^2]$$

or

$$T_0^{calc(\mu_0 H_{ext})} = \tfrac{1}{2}V_0\omega\mu_0 H_{ext}C_{eff}(r_2^2-r_1^2) \tag{4}$$

with

$$C_{eff} = C_{vac}+\frac{1}{2}\frac{C_2\hat{r}_2^2-C_1\hat{r}_1^2}{r_2^2-r_1^2}. \tag{5}$$

From a general point of view, the analysis of the complete set of forces acting on S starts by considering the total localised phenomenological force density according to its orthodox expression and according to the (updated) Livens proposal (Lahoz and Graham 1981, formulae (11) and (16)). In this experiment $\mu_0 H_{ext}$ = constant and the dielectric in V is a magnetic material; thus the only terms of the force density expressions which could contribute a measurable torque are

$$\boldsymbol{f}_{orth} = (\boldsymbol{j}+\dot{\boldsymbol{P}})\times\mu_0\boldsymbol{H}+\mu_0\boldsymbol{M}\cdot\nabla\boldsymbol{H}, \tag{6}$$

$$\boldsymbol{f}_{Livens} = (\boldsymbol{j}+\dot{\boldsymbol{P}})\times\boldsymbol{B}+M_j\nabla B_j. \tag{7}$$

Disregarding the localisation key in order to obtain the net torque on S, we transform the Kelvin term as follows:

$$\mu_0\boldsymbol{M}\cdot\nabla\boldsymbol{H} \equiv \mu_0 M_j\nabla H_j - \boldsymbol{M}\times(\nabla\times\mu_0\boldsymbol{H}) = \mu_0 M_j\nabla H_j+(\boldsymbol{j}+\dot{\boldsymbol{P}})\times\mu_0\boldsymbol{M}+\varepsilon_0\dot{\boldsymbol{E}}\times\mu_0\boldsymbol{M},$$

and noticing that the azimuthal components of $\mu_0 M_j\nabla H_j$ and $M_j\nabla B_j$ are zero for our geometry (figure 1), the relevant force density terms become

$$\boldsymbol{f}_{orth} = (\boldsymbol{j}+\dot{\boldsymbol{P}})\times\boldsymbol{B}+\varepsilon_0\dot{\boldsymbol{E}}\times\mu_0\boldsymbol{M}, \tag{8}$$

$$\boldsymbol{f}_{Livens} = (\boldsymbol{j}+\dot{\boldsymbol{P}})\times\boldsymbol{B}. \tag{9}$$

The quantity $\boldsymbol{j}=\boldsymbol{j}_{\dot{P}}+\boldsymbol{j}_{\dot{E}}+\boldsymbol{j}_2+\boldsymbol{j}_1$ represents the total conduction current elements running horizontally in the radial leads R and vertically in part of the plates P_2 and P_1; $\boldsymbol{j}_{\dot{P}}$ completes closed loops as polarisation current in the dielectric V; $\boldsymbol{j}_{\dot{E}}$ does the same as vacuum displacement current in V; $\boldsymbol{j}_2$ is a set of current elements $\overline{def}$ through R, then through the outer surface of P_2, and finding their way out of S as vacuum displacement currents through C_2 to G_2; finally, $\boldsymbol{j}_1$ stands for the return conduction current elements

$\overline{npq}$ which are the continuation of vacuum displacement currents through C_1 (from G_1 to P_1). The remaining azimuthal conduction current elements in plates P_2 and P_1 or in the filaments F do not need to be considered since they do not impart measurable torques on S for obvious reasons.

The next step in our analysis is to recall the torque theorem (Lahoz and Graham 1979a) in order to simplify (8) and (9): the net torque on S caused by the magnetic material in V (equivalent to a set of azimuthal currents) in interaction with any closed vertical loop of conduction and polarisation currents is zero. Therefore, if $\mu_0 H^M$ is the magnetic field caused by the magnetic material in V,

$$\boldsymbol{B} = \mu_0 \boldsymbol{H}_{\text{ext}} + \mu_0 \boldsymbol{H}^M + \mu_0 \boldsymbol{M}, \tag{10}$$

the terms

$$(\boldsymbol{j}_{\dot{P}} + \dot{\boldsymbol{P}}) \times \boldsymbol{B} = (\boldsymbol{j}_{\dot{P}} + \dot{\boldsymbol{P}}) \times \mu_0 \boldsymbol{H}_{\text{ext}} + (\boldsymbol{j}_{\dot{P}} + \dot{\boldsymbol{P}}) \times \mu_0 \boldsymbol{H}^M + \dot{\boldsymbol{P}} \times \mu_0 \boldsymbol{M} \tag{11}$$

can be dropped in (8) and (9) as they will integrate to torques on closed vertical loops. Using the fact that all conduction currents are external to V (an insulator), i.e. j is zero wherever $\boldsymbol{M} \neq 0$, naming $\boldsymbol{E}^V$ the $\boldsymbol{E}$ field within V and noticing that the terms $(\boldsymbol{j}_{\dot{E}} + \varepsilon_0 \dot{\boldsymbol{E}}^V) \times \mu_0 \boldsymbol{H}^M + \varepsilon_0 \dot{\boldsymbol{E}} \times \mu_0 \boldsymbol{M}$ give no contribution since their net effect is equal to forces on systems of closed vertical conduction current loops, the relevant force density terms acting on S can be collected as

$$\boldsymbol{f}_{\text{orth}} = (\boldsymbol{j}_{\dot{E}} + \boldsymbol{j}_2 + \boldsymbol{j}_1) \times \mu_0 \boldsymbol{H}_{\text{ext}} + (\boldsymbol{j}_2 + \boldsymbol{j}_1 - \varepsilon_0 \dot{\boldsymbol{E}}^V) \times \mu_0 \boldsymbol{H}^M, \tag{12}$$

$$\boldsymbol{f}_{\text{Livens}} = (\boldsymbol{j}_{\dot{E}} + \boldsymbol{j}_2 + \boldsymbol{j}_1) \times (\mu_0 \boldsymbol{H}_{\text{ext}} + \mu_0 \boldsymbol{H}^M) = \boldsymbol{f}_{\text{orth}} + (\varepsilon_0 \dot{\boldsymbol{E}}^V + \boldsymbol{j}_{\dot{E}}) \times \mu_0 \boldsymbol{H}^M, \tag{13}$$

which clearly show that the torque due to $\mu_0 H_{\text{ext}}$ is common to both theories and is given by (4). The terms proportional to $\mu_0 H^M$ in (12) generate the following torque amplitude:

$$T_{0\,\text{orth}}^{\text{calc}(\mu_0 H^M)} = \left| \mu_0 \int_0^{r_2} r \, \mathrm{d}r \int_{-h/2}^{h/2} i_2 \hat{H}_z^M(r, z) \, \mathrm{d}z - \mu_0 \int_0^{r_1} r \, \mathrm{d}r \int_{-h/2}^{h/2} i_1 H_z^M(r, z) \, \mathrm{d}z \right.$$
$$\left. + \mu_0 \int_{r_1}^{r_2} r \, \mathrm{d}r \int_{-h/2}^{h/2} i_{\text{vac}} H_z^M(r, z) \, \mathrm{d}z \right|. \tag{14}$$

In these integrals the current densities i_2, i_1 and i_{vac} are constant and given by

$$i_2 = (1/2h)\omega C_2 V_0, \qquad i_1 = (1/2h)\omega C_1 V_0, \tag{15}$$

$$i_{\text{vac}} = (1/h)\omega C_{\text{vac}} V_0 \tag{16}$$

where $\frac{1}{2}V_0$ is the voltage amplitude between plate P_2 and ground G_2 (or plate P_1 and G_1). Note also that we have again used the torque theorem to replace the actual conduction current elements $\overline{def}$ (figure 1) by equivalent horizontal conduction current elements $\overline{gf'f}$ in the first integral; similarly the conduction currents $\overline{npq}$ have been replaced by horizontal conduction current elements $\overline{nm}$ in the second (negative) integral. Correspondingly the $\mu_0 H^M$ field has also been replaced by the field $\mu_0 \hat{H}^M$ caused by two coaxial antiparallel solenoids with equal amount of magnetic excitation, $|ni/l|$, such that $\mu_0 H^M \simeq \mu_0 \hat{H}^M$ outside V. Within V one clearly has

$$\mu_0 \hat{H}_z^M(z) \simeq B_z^M \equiv \mu_0 H_z^M(z) + \mu_0 M_z \tag{17}$$

where the magnetisation of the sample, $\boldsymbol{M}(z) \simeq M_z \boldsymbol{k}$, is being considered as constant (>0, say) and along the $0z$ axis within V. The demagnetising field $\mu_0 H^M(z)$ is opposed

to $\mu_0 M$ within V and we will assume that $\mu_0 H^M(0) \simeq 0$. These approximations are clearly adequate when our long and/or thin samples are saturated and still reasonable even at low excitations $\mu_0 H_{\text{ext}}$ (when an exact calculation of the enhancement of $\mu_0 M$ at the edges of the cylinder V would be cumbersome and unnecessary for our purposes).

A computer program for the current density approach (replacement of the ferrite by two antiparallel coaxial solenoids) gave a substantially flat function of r, $\mu_0 \hat{H}_z^M(r, z_0)$, for any $z = z_0$ within V for the geometry of our samples. Therefore we will assume for our cases:

(a) within V:

$$\mu_0 \hat{H}_z^M(r, z) \simeq \mu_0 \hat{H}_z^M(z) \simeq \mu_0 M_z + \mu_0 H_z^{M(\text{in})}(z); \tag{18}$$

(b) outside V:

$$|\mu_0 \hat{H}_z^M| = |\mu_0 H_z^{M(\text{out})}(r, z)| \leqslant |\mu_0 H_z^{M(\text{in})}(z)|. \tag{19}$$

Substitution of (19), (18), (16) and (15) in (14) gives:

$$\begin{aligned} T_{0\,\text{orth}}^{\text{calc}(\mu_0 H^M)} = \Big| & \tfrac{1}{4}\omega V_0 C_2 (r_2^2 - r_1^2) \int_{-h/2}^{h/2} \mu_0 \hat{H}_z^{M(\text{in})}(z) \frac{\mathrm{d}z}{h} \\ & + \tfrac{1}{4}\omega V_0 r_1^2 (C_2 - C_1) \int_{-h/2}^{h/2} \mu_0 \hat{H}_z^{M(\text{out})}(z) \frac{\mathrm{d}z}{h} \\ & + \tfrac{1}{2}\omega V_0 C_{\text{vac}} (r_2^2 - r_1^2) \int_{-h/2}^{h/2} (\mu_0 \hat{H}_z^{M(\text{in})}(z) - M_z) \frac{\mathrm{d}z}{h} \Big|. \end{aligned} \tag{20}$$

The remaining integrals are simple averages of the two-solenoid field. Introducing a demagnetisation parameter δ (see table 1), we write the first integral as

$$\int_{-h/2}^{h/2} \hat{H}_z^{M(\text{in})}(z) \frac{\mathrm{d}z}{h} = \delta \mu_0 M_z \qquad (\delta < 1) \tag{21}$$

whereas the second, using (19) and (18), has an absolute value smaller than $(1-\delta)\mu_0 M_z$ and consequently

$$T_{0\,\text{orth}}^{\text{calc}(\mu_0 H^M)} = \tfrac{1}{2}\omega V_0 (r_2^2 - r_1^2) \mu_0 M_z [\tfrac{1}{2}\delta C_2 (1+\eta) - (1-\delta) C_{\text{vac}}] \tag{22}$$

with

$$|\eta| < (1-\delta)|1 - C_1/C_2|/\delta[(r_2/r_1)^2 - 1]. \tag{23}$$

In all the cases to be discussed in this report, $|\eta| < 0.1$. It represents less than a 10% correction to a small quantity (see § 5); thus we will set $\eta \simeq 0$ from now on.

Finally the torque induced by the terms $(\varepsilon_0 \dot{\boldsymbol{E}}^{\text{V}} + \boldsymbol{j}_{\dot{E}}) \times \mu_0 \boldsymbol{H}^M$ in (13) is easily obtained with the aid of the torque theorem: we can replace the actual paths $\overline{def}$ and $\overline{f'f''d}$ (figure 1) of conduction current elements ($\boldsymbol{j}_{\dot{E}}$) by horizontal conduction current elements $\overline{f'f}$ acted by $\mu_0 M_z + \mu_0 H^{M(\text{in})}$. Hence

$$T_{0\,\text{Livens}}^{\text{calc}(\mu_0 H^M)} = T_{0\,\text{orth}}^{\text{calc}(\mu_0 H^M)} + \mu_0 \int_{r_1}^{r_2} r\,\mathrm{d}r \int_{-h/2}^{h/2} \omega C_{\text{vac}} V_0 M_z \frac{\mathrm{d}z}{h}. \tag{24}$$

Using (22) we obtain

$$T_{0\,\text{orth}}^{\text{calc}(\mu_0 H^M)} = \tfrac{1}{2}\omega V_0 \mu_0 M_z (r_2^2 - r_1^2)[\tfrac{1}{2}\delta C_2 - (1-\delta) C_{\text{vac}}], \tag{25}$$

$$T_{0\,\text{Livens}}^{\text{calc}(\mu_0 H^M)} = \tfrac{1}{2}\delta\omega V_0 \mu_0 M_z (r_2^2 - r_1^2)(\tfrac{1}{2} C_2 + C_{\text{vac}}), \tag{26}$$

and adding these contributions to (4) and defining B^{eff} from

$$T_0 \equiv \tfrac{1}{2}(r_2^2 - r_1^2) C_{\text{eff}} \omega V_0 B^{\text{eff}} \tag{27}$$

we have, in summary,

$$B^{\text{eff}}_{\text{orth}} = \mu_0 H_{\text{ext}} + \frac{\delta C_2 - 2(1-\delta) C_{\text{vac}}}{2 C_{\text{eff}}} \mu_0 M_z, \tag{28}$$

$$B^{\text{eff}}_{\text{Livens}} = \mu_0 H_{\text{ext}} + \frac{\delta (C_2 + 2 C_{\text{vac}})}{2 C_{\text{eff}}} \mu_0 M_z, \tag{29}$$

$$B^{\text{eff}}_{\text{meas}} = \frac{2 T_0^{\text{meas}}}{(r_2^2 - r_1^2) C_{\text{eff}} \omega V_0} = \frac{4 I \alpha_\infty}{(r_2^2 - r_1^2) C_{\text{eff}} V_0 \tau}. \tag{30}$$

The last equality follows from

$$T_0^{\text{meas}} = (2 \omega I / \tau) \alpha_\infty \tag{31}$$

where T_0^{meas}, the measured torque amplitude, is obtained as in our previous experiments (Lahoz and Graham 1979a, Graham and Lahoz 1981). I, τ and α_∞ are the inertia moment, the time constant and the steady state amplitude of angular displacement of the torsional pendulum, respectively.

3. Technical description of the experiment

The set-up of the present experiment does not differ essentially from that of our previous measurement of electromagnetic momentum in a vacuum ring. In particular, the torque measurement apparatus has been thoroughly described there as a resonant torsional pendulum in which the 'load' is a cylindrical capacitor with radial leads tightly clamped to the suspension (Graham and Lahoz 1980, figure 1). Two differences have to be mentioned. (a) The capacitance vacuum gap is now filled with a magnetic material as part of the load (the system S described in § 1). This increases the inertia moment but simplifies the clamping of the load. (b) The magnetic hysteresis loop associated with the magnetic material imposes limitations on the use of the 'breathing' B field. This technique (in which the B field is sinusoidally varied at ~ 0.3 Hz) was eventually abandoned for the present situation after some unsuccessful trials. Furthermore, the strong magnetic moment on the load of the pendulum generates lateral forces, due to unavoidable slight inhomogeneity of the $\mu_0 H_{\text{ext}}$ field, and the time constant τ of the suspension is now liable to small erratic changes (after a reversal of $\mu_0 H_{\text{ext}}$, say) induced by minute tiltings of the torsion shaft.

These differences recommended the use of very thin shells of ferrite, as dielectric, in compromise with mechanical integrity (figure 2) and electrical insulation properties; the $\mu_0 H_{\text{ext}}$ was kept constant during each measurement. A DC power supply (6260B Hewlett–Packard) fed, through a $\sim 0.1\ \Omega$ stabilising resistor and superconducting leads supported by heavy stainless-steel ingots, a long (~ 10 cm) superconducting coil C ($L \simeq 0.2$ H), placed in a He dewar (Lahoz and Graham 1979a, figure 1). The $\mu_0 H_{\text{ext}}$ could easily be reversed and controlled up to 3 T with small departures ($\leqslant 5\%$) from homogeneity within a long vacuum cylinder (~ 5 cm) confined by a thin stainless-steel pipe of radius $t \simeq 1.6$ cm (figure 1).

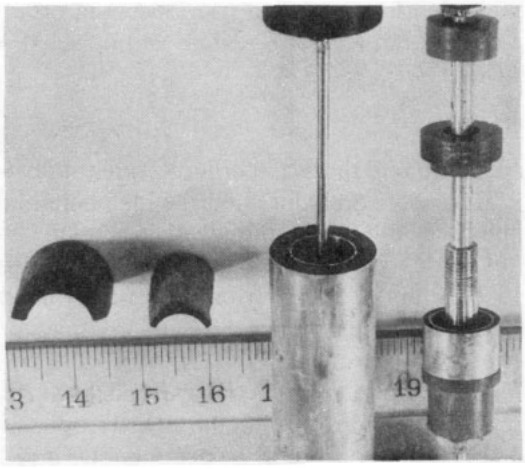

Figure 2. The four samples which have yielded results. From left to right: a portion of the sintered magnetite used in the first work (Lahoz and Graham 1979b), part of the (Ni–Zn)-ferrite sample and the natural magnetite specimen and the Ba-ferrite sample with their respective suspensions.

3.1. The noise problem and the injection of subharmonic voltage

The basic hindrance in all these measurements (Lahoz and Graham 1979a) is noise at frequency ω: the rest of the noise spectrum is efficiently wiped out by the $Q \simeq 10^5$ of the torsional pendulum. The resonant noise is essentially generated by moving mechanical elements associated with the wiring which feed the capacitor plates. Thus it is inherent to the very nature of the experiment and only in lucky instances (one out of ten trials, say) is the net effect of these acoustical noises *per se* stable and negligible. The control of this E^2 noise becomes eventually the main goal in all these experiments. Graham and Lahoz (1981) have described two noise-controlling methods; the 'breathing' B technique (not applicable here) and the injection of subharmonic voltage. The development of this last method in the present experiment constitutes the major improvement with respect to the preliminary work (Lahoz and Graham 1979b).

Although the E^2 noise, being proportional to $(V_0 \sin \omega t)^2 = \frac{1}{2}V_0^2(1 - \cos 2\omega t)$, originates at frequency 2ω in the wiring, low-order harmonics and subharmonics are concomitantly produced by nonlinear mechanisms in these hidden transducers and the Fourier component at frequency ω reaches the pendulum with phase and amplitude which either varies randomly in short periods of time (~5 minutes), rendering the whole apparatus useless, or, more frequently (taking sensible precautions, such as extreme care in straightening the fibres F, figure 1), the E^2 noise pattern is relatively stable in phase and amplitude. These normal situations are identified by observed traces in the CRO, due to an injected input V_0 (with $B = 0$ or $B \neq 0$), which remain constant with stable phase and amplitude in the long range of time (hours). We obviously interpret these last symptoms as an indication that the hidden transducers are far away from critical (unstable) working points and then, in addition to the voltage $V(t) = V_0 \sin \omega t$ responsible for the torque to be measured, we inject into the wiring a subharmonic voltage $V_s(t) = V_s^0 \sin(\frac{1}{2}\omega t + \phi_s)$, such that the added electromagnetic forces in the load, at frequency $\omega/2$, are essentially rejected by the large Q of the suspension and do not interfere with the measurement of the electromagnetic torque. The intended side effect

is to provide a combined excitation to the hidden transducers in order to generate a combined acoustical effect: the normal E^2 noise and an 'antinoise' A at frequency ω and proportional to $[V_s^0 \sin(\frac{1}{2}\omega t + \phi_s)]^2$:

$$A = A_0 \cos(\omega t + 2\phi_s). \tag{32}$$

The response of a torsional pendulum to these and other torques has been discussed by Graham and Lahoz (1981). Here we merely insist on the idea behind this technique: one can arbitrarily manipulate the phase and amplitude of V_s until the ω component of the E^2 noise and 'antinoise' (32) add to zero. We found that a few readjustments of the subharmonic during the 8 to 24 hours of a single run were usually needed in order to track small variations of the E^2 noise pattern. Thus the standard (final) procedure starts with a preliminary observation of a reproducible trace in the CRO, $T_0 + N \exp(i\phi_N)$, with stable noise amplitude N and phase ϕ_N, which by reversing the B field (going to $\mu_0 H_{ext} \simeq 3$ T and coming back from saturation to the exactly opposite value of B) becomes $-T_0 + N \exp(i\phi_N)$ (since the noise term is, presumably, independent of the sign of the B field). Then, by successive trial-and-error injections of subharmonic, the signal T_0 is purified until N is so small that the CRO trace merely undergoes a 180° shift at sensibly constant amplitude after a B reversal. A small noise component in quadrature to the signal ($\phi_N = \pm\pi/2$) is usually almost unavoidable and does not represent a large inconvenience, but when N is large the extraction of the signal T_0 from the half-difference of the traces at both signs of the B field yields erratic results due to minor phase shifts of the noise and other complications. Thus the data presented as final in this report correspond to a selection of those runs which gave symmetrical trace under B reversal or negligible trace in the limit $\mu_0 H_{ext} = 0$.

3.2. Electronic circuitry

The frequency ω of the electromagnetic torque applied to the system S is kept identical to the resonant frequency of the pendulum, and their phase difference is also maintained, measured and controlled by means of the usual feedback system common to all our previous experiments. The E field power supply for the present case is fully described in figure 3. The main innovation can be described as follows: the optional injection of subharmonic is presently derived from the same voltage-controlled oscillator which generates the main input at frequency ω; the monitor output of the PAR (figure 3) yields directly a clean sine wave S at frequency $\omega/2$. We found that the phase and volume control of the subharmonic is extremely critical and time-consuming during the actual measurements.

4. The magnetic samples and their suspensions

Three different types of ferrite were used in the present experiment: they were adequate for discriminating f_{Livens} from f_{orth} in different ranges of the B field. The samples were mounted in corresponding suspensions machined, as a single piece, from Al–bronze of the 2024 type (4.4% Cu, 1.6% Mg, 0.6% Mn) for the Fe_3O_4 sample and of the 2011 type (5.5% Cu, 0.4% Pb, 0.4% Bi) for the other two samples. Both alloys have very low internal friction at ~4.2 K, the Q of the suspensions ranging from 10^4 (in high fields) up to 4×10^5. In figure 2 we present a photograph of all the samples which have been used for this experiment including our preliminary work. Relevant technical

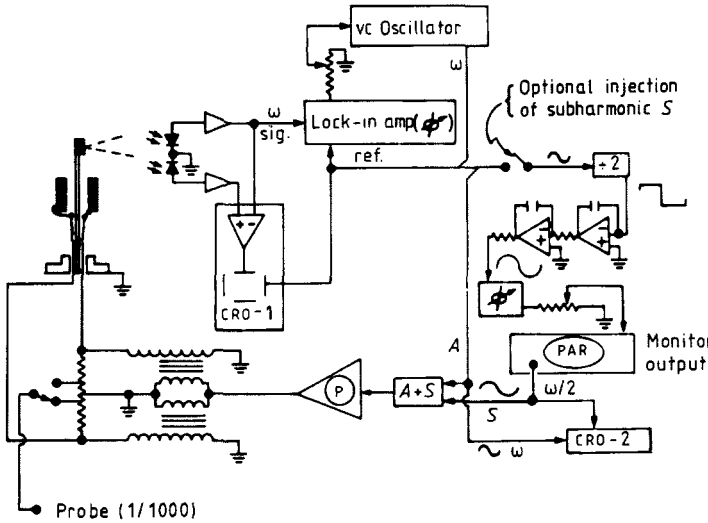

Figure 3. Electronic elaboration of the signal and power supply for the E field input. PAR: gain and filter sections of lock-in amplifier (HR-8 Princeton Appl. Res.). P: AC power amplifier (PA 250-optimation).

data for the samples are collected in table 1. The work with the (Ni–Zn)-ferrite was done about two years ago in a few runs before the sample split under low-temperature stresses. The electronic circuitry (at that time) differed slightly from that in figure 3: it had no option for subharmonic injection and the inner plate P_1 (figure 1) was connected to ground (G_1 and G_2). Thus the corrections due to C_1, C_2 and C_{eff} as presented in § 2 have to be modified for this case in an obvious manner (replacing $\frac{1}{2}C_2$ by C_2 and setting $C_1 = 0$ in (5), (25) and (26)). The last two samples were mechanically protected with

Table 1. Dimensions and parameters of the samples in their suspensions.

Sample	(Ni–Zn)-ferrite	Natural magnetite	Ba-ferrite
Outside radius, r_2 (cm)	0.49	0.73	0.55
Inside radius, r_1 (cm)	0.395	0.49	0.48
Length, h (cm)	2.36	4.63	0.72
Density, ρ (g cm^{-3})	4.2	5.13	4.8
Capacitance at ~200 Hz (pF)	~70	~325	~50
$RC\omega$ at ~4.2 K	$>10^4$	~70	~6000
Demagnetisation parameter, δ	~0.95	~0.93	~0.91
Vacuum capacitance, C_{vac} (pF)	6.02	6.6	2.96
Leak capacitance to G_2, C_2 (pF)	~1.2	~3.8	~0.4
Leak capacitance to G_1, C_1 (pF)	—†	~3.5	~0.7
Outer radius of plate P_2, $\hat{r}_2$ (cm)	0.49	0.75	0.57
Inner radius of plate P_1, $\hat{r}_1$ (cm)	0.39	0.44	0.43
Effective vacuum capacitance, C_{eff} (pF)	9.5†	9.1	2.97
Inertia moment, I (g cm^2)	0.7	12.5	0.82
Resonance frequency at ~4.2 K, $\omega/2\pi$ (Hz)	156.2	124.53	271.35

† See specifications in the text.

cylindrical brass shells, firmly attached to the magnetic specimens with conductive glue and acting as plates P_1 and P_2 of the capacitor. Of crucial interest for the experiment are the magnetisation curves of the three kinds of materials: they are presented in figure 4 as combined results of our direct measurements and information extracted from the literature.

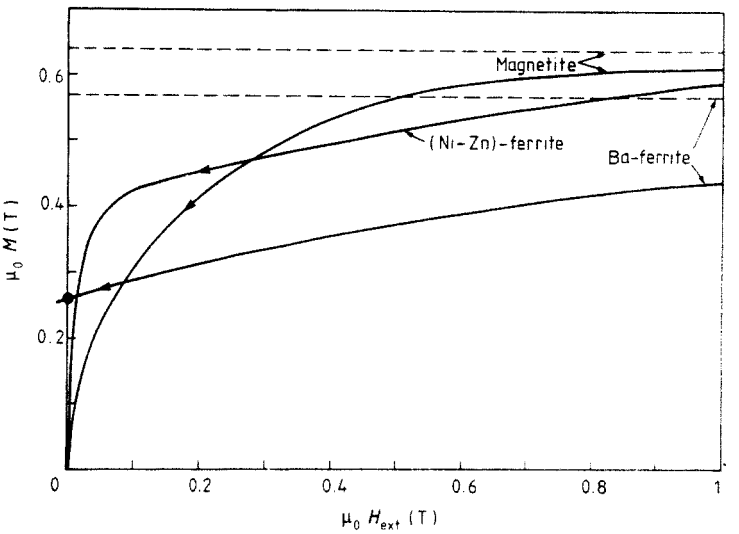

Figure 4. Magnetisation curves at ~4.2 K of the three magnetic materials used in the experiment.

4.1. (Ni–Zn)-ferrite sample

This was a well machined cylindrical shell of sintered ferrite intended for commercial RF application with high initial permeability at room temperature similar to Ferroxcube 4A. Its approximate composition, $(NiO)_{0.3}(ZnO)_{0.7}Fe_2O_3$, was determined by semiquantitative chemical analysis complemented with measurement of the Curie point (~380 K) and temperature dependence of the hysteresis cycle and initial permeability. A study of these ferrites by Pauthenet (1952, pp 738–41) predicts for our sample a saturation magnetisation $\mu_0 M_{sat} \simeq (0.65 \pm 0.05)$ T at large excitations $\mu_0 H_{ext} \simeq 2$ T and a knee of the curve (extrapolated) at $\mu_0 H_{ext} \simeq 0.2$ T. Our measurements confirmed these results both at room temperature and at ~4.2 K when using maximal excitation of 0.3 T and 1.2 T, respectively. However, using a toroidal specimen Stuijts *et al* (1964) have found magnetisation curves with a knee at $\mu_0 H_{ext} \simeq$ 0.0005 T for similar materials and, in fact, we also obtained hysteresis loops (for toroidal geometry) consistent with this, but only when the maximal excitations were $\mu_0 H_{ext} \simeq 0.002$ T (as is the case in ordinary applications). This seemingly bizarre discrepancy can probably be explained, taking into consideration Pauthenet's remarks: for these ferrites with high Zn percentage the magnetisation curve grows steadily (almost linearly) and it is difficult to reach the saturation (at $\mu_0 H_{ext} > 2$ T). In any case the relevant magnetisation curve for our experiment ($\mu_0 H_{ext}^{max} \simeq 1.2$ T) at ~4.2 K was directly measured and is presented in figure 4. The remanence, $\mu_0 M_{rem}$, was neglected in this case since measurements with our specific sample gave values $\leqslant 0.002$ T.

4.2. Natural magnetite sample

This was drilled out of high-purity polycrystalline rock from Espanola (Ontario), courtesy of Professor D H Gorman (Department of Geology), and machined afterwards as a single piece. Taking into consideration the measured density of 5.13 g cm^{-3}, we derived its corresponding magnetisation curve at ~4.2 K using the following information from the literature: (a) Jacobs (1959) gives a magnetisation curve for Fe_3O_4 (powder) at 4.2 K; (b) detailed magnetisation curves presented by Domenicali (1950) and Calhoun (1954) for single crystals (with field along different axes) below the transition temperature are consistent with Jacob's results and with a saturation value $\mu_0 M_{sat} \simeq 0.63$ T (in the density range relevant to our case); (c) no remanence has been assumed: it was observed to be minimal at room temperature, and data of Domenicali (1950) show the same when, as in our case, the specimen is cooled at $B \simeq 0$. The result of this compilation is presented in figure 4.

The usual small net force (not torque!) on the load due to unequal length of the two radial conductors R (figure 1) cannot generate sensible effects since it is out of resonance for causing pendular motion; however it could, as a remote possibility, interact with incidental axial asymmetries in the suspension and produce an unwanted resonant torque. This possibility was eliminated in this case by using four 1 kΩ tiny carbon resistors (replacing the radial leads R) in order to distribute the conduction currents in four axially symmetric paths (from fibres F near the axis to two opposite points in each plate of the capacitor). This is probably a redundant precaution which was not taken for the other samples.

4.3. Ba-ferrite sample

This was machined from a commercial permanent magnet (sintered ferrite). Quantitative chemical analysis gave an approximate composition $BaFe_{12}O_{19}$. The remanence was measured at 20 °C, $\mu_0 M_{rem} \simeq 0.19$ T, in agreement with Flanders and Shtrikman (1962). The ratio of the saturation and remanence values for these ferrites $M_{sat}/M_{rem} \simeq 2.1$ is approximately independent of the temperature (Smit and Wijn 1960). $\mu_0 \boldsymbol{M}_{sat}$ does not follow a Langevin curve in its temperature dependence. From published data of $\mu_0 M_{sat}$ as a function of temperature (Richter and Dietrich 1968), we conclude that for our sample

$$\mu_0 M_{rem} = 0.27 \text{ T}, \qquad \mu_0 M_{sat} \simeq 0.57 \text{ T} \qquad (\text{at } \sim 4.2 \text{ K}). \tag{33}$$

Using a thin and long rod of this material, we measured the actual magnetisation curve at ~4.2 K up to $\mu_0 H_{ext} \simeq 1.2$ T. The outcome, consistent with (33), is presented in figure 4.

5. Results

From (5), (28), (29) and table 1 the theoretically predicted curves $B^{eff}_{orth}(\mu_0 H_{ext})$ and $B^{eff}_{Livens}(\mu_0 H_{ext})$ become (for our three samples in the sequence (Ni–Zn)-ferrite, magnetite and Ba-ferrite):

$$B^{eff}_{orth} = \mu_0 H_{ext} + \left\{ \begin{matrix} 0.09 \\ 0.14 \\ -0.03 \end{matrix} \right\} \mu_0 M_z(\mu_0 H_{ext}), \tag{34}$$

$$B^{\text{eff}}_{\text{Livens}} = \mu_0 H_{\text{ext}} + \begin{Bmatrix} 0.81 \\ 0.87 \\ 0.97 \end{Bmatrix} \mu_0 M_z(\mu_0 H_{\text{ext}}), \tag{35}$$

where the functions $\mu_0 M_z(\mu_0 H_{\text{ext}})$ are graphically given (for each sample) in figure 4. The curves (34) and (35) are plotted in figures 5, 6, 7. The corresponding measured quantities $B^{\text{eff}}_{\text{meas}}(\mu_0 H_{\text{ext}})$, as derived from (30) and table 1, are

$$B^{\text{eff}}_{\text{meas}} = \begin{Bmatrix} 0.37 \\ 1.85 \\ 1.53 \end{Bmatrix} \times 10^{10} \frac{\alpha_\infty}{V_0 \tau}. \tag{36}$$

For a given voltage amplitude V_0 the quantities α_∞ and τ are functions of $\mu_0 H_{\text{ext}}$ and were obtained by lengthy measuring processes which deserve some specific comments.

5.1. Early measurements with the (Ni–Zn)-ferrite sample

Due to the relatively large initial permeability (even at low temperatures) of this sample, (34) and (35) show a marked discrepancy at extremely low magnetic excitations $\mu_0 H_{\text{ext}}$, and a good discrimination is therefore possible. At the time of these measurements, the subharmonic injection device was not yet available, but we carried out one particularly noiseless run (at a fixed V_0 value, which unfortunately was not properly

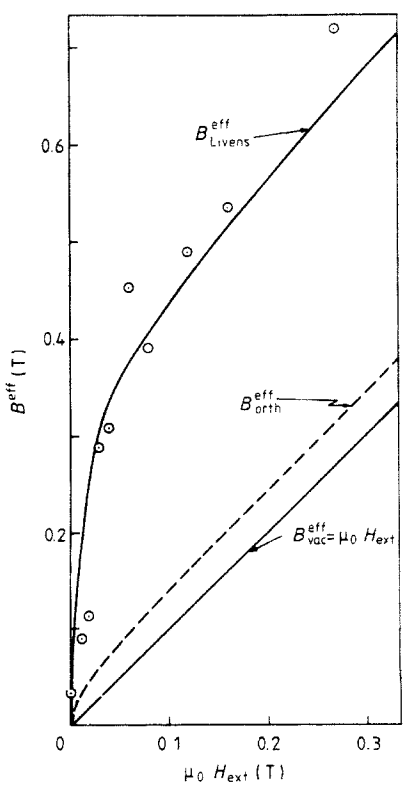

Figure 5. The (Ni–Zn)-ferrite results. ⊙ $B^{\text{eff}}_{\text{meas}}$ (14.3.1979).

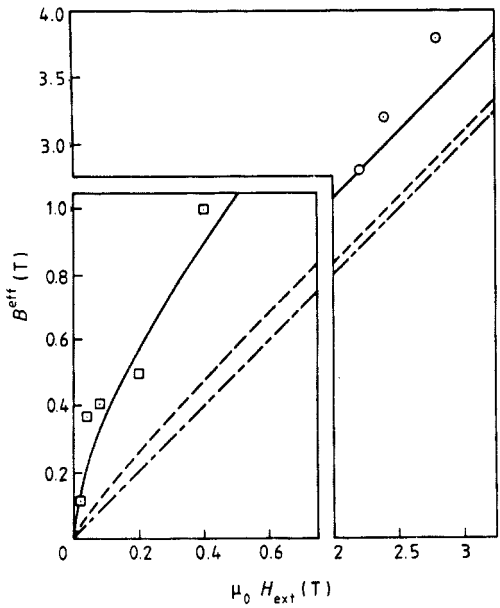

Figure 6. Results with the natural magnetite sample. ——— $B^{eff}_{vac} = \mu_0 H_{ext}$, --- B^{eff}_{orth}, —— B^{eff}_{Livens}, ⊙ B^{eff}_{meas} (12.12.1980) ⊡ B^{eff}_{meas} (30.12.1980).

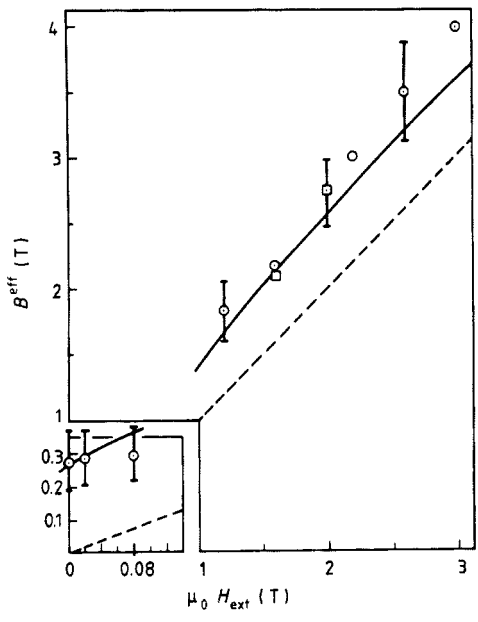

Figure 7. Final results with the Ba-ferrite sample. ⊙ B^{eff}_{meas} (10.1.1981), ⊡ B^{eff}_{meas} (25.1.1981), --- $B^{eff}_{orth} \simeq \mu_0 H_{ext}$, —— B^{eff}_{Livens}.

recorded due to a faulty probe): we swept (without reversal) the $\mu_0 H_{ext}$ field down to its lowest values. Since $1/\tau$ is proportional to $(\mu_0 H_{ext})^2$ (Graham and Lahoz 1981), the noise component in the observed steady state traces of the CRO usually tended to become large at $B \simeq 0$; during this particular run that trace was practically zero at the expected phase for the signal: the criterion for a noiseless run was fulfilled (§ 3) and the eleven points of the run were considered outstanding measurements. The unrecorded parameter V_0 is estimated as follows. The first point of the run (not shown in figure 5) at a large magnetic excitation $\mu_0 H_{ext} = 1.2$ T had the smallest *a priori* probable error, since the signal-to-noise ratio tends to be proportional to $1/\tau$; thus, assuming that it fitted exactly the corresponding $B^{eff}_{Livens} \simeq 1.7$ T and using the measured quantities $\alpha_\infty \simeq 13 \times 10^{-6}$ rad, $\tau = 92$ s, we derived $V_0 \simeq 309$ V as the missing parameter; this V_0 value was inserted into (36) (with its top factor 0.37) and the remaining ten points of the run became fully determined and are plotted in figure 5. These data show a remarkably good overall agreement with B^{eff}_{Livens} and are definitively inconsistent with the quasi-linear contender $B^{eff}_{orth}(\mu_0 H_{ext})$. Incidentally, the observed sharp bending of $B^{eff}_{meas}(\mu_0 H_{ext})$ near the origin was the chief motivation for our detailed revision of the phenomenological force density from a theoretical point of view (Lahoz and Graham 1981).

5.2. Measurements with magnetite

The three points at large $\boldsymbol{B}$ fields (figure 6) were obtained without subharmonic injection using the advantages of low τ (from 20 to 11 s): enhancement of the signal-to-noise ratio. They were reasonably symmetrical on reversal of $\mu_0 H_{ext}$: each

point represents a pair of equivalent measurements at opposite $\boldsymbol{B}$ fields. The deviations from $B^{\text{eff}}_{\text{Livens}}$ can be attributed, in part, to erratic contributions of mechanical noise, since the working frequency (~124 Hz) was exceedingly low and the suspension picked up, by small kicks, the inefficiently filtered lower band of the ambiental noise spectrum. After recognition of this fact, we performed other measurements at night with consistently lower dispersion and, in particular, the five double points at low $\pm B$ field values as plotted in figure 6. These $B^{\text{eff}}_{\text{meas}}$ points were highly symmetric and convergent at the origin thanks to the use of subharmonic injection during this 24 hour run. A double point at $\mu_0 H_{\text{ext}} = \pm 0.6$ T, $B^{*\text{eff}}_{\text{meas}} \simeq 1.4\, B^{*\text{eff}}_{\text{Livens}}$ (not shown in figure 5), was checked the next day (without subharmonic), yielding again $B^{*\text{eff}}_{\text{meas}} \simeq 1.3\, B^{*\text{eff}}_{\text{Livens}}$; this is an oddity which could be understood as an experimental artifact at this particular value of $\mu_0 H_{\text{ext}}$ (the maximum usable in these last runs with the magnetite sample after an unfortunate bending of the torsional shaft which drastically reduced the τ values). Thus, despite the small number of adequate measurements, the results again favour the Livens theory and cannot be considered consistent with $B^{\text{eff}}_{\text{orth}}$.

5.3. Final measurements with the Ba-ferrite sample

With the aid of the subharmonic injection, we managed to obtain a 20 hour run which included both large and extremely low magnetic excitations (figure 7). The τ (in seconds) for this run closely followed the typical dependence relationship with $\mu_0 H_{\text{ext}}$ (in T): $\tau = 167/[0.257 + (\mu_0 H_{\text{ext}})^2]$. The most noteworthy results are the three double points at $\mu_0 H_{\text{ext}} = (\pm 0.072, \pm 0.020, \pm 0.000)$ T. They were reasonably symmetric under reversal of the B field, which, even at $\mu_0 H_{\text{ext}} = \pm 0.000$ T, meant a forward and back sweep up to 3 T in order to ensure the reversal of $\mu_0 M_{\text{rem}} \simeq 0.27$ T. These three double points conclusively rule out the adequacy of the orthodox theory predicting a ~0 value and, within the relatively large experimental errors, they fit well the theoretical values of the Livens theory. It is, perhaps, enlightening to remark that for $\mu_0 H_{\text{ext}} \geqslant 0$ the signal (practically equal, in this case, to the CRO trace) kept its constant phase all the way from $B \simeq +(3 + 0.57)$ T down to $B \simeq +(0 + 0.27)$ T, in agreement with the Livens prediction. $B^{\text{eff}}_{\text{orth}}$, on the other hand, reverses its sign at $\mu_0 H_{\text{ext}} \simeq +0.008$ T (see (34)), predicting a 180° phase shift in the CRO trace which was not observed.

The same conclusion follows from the seven pairs of points at large $\pm B$ fields in spite of ~14% error bars. These large errors appear to be inherent in this experiment, which, if not fully adequate for accurate evaluations of B^{eff}, does certainly deny to the orthodox theory the right to be considered as a valid alternative.

6. Conclusion

Taking into consideration the fact that the orthodox theory has been widely trusted for more than half a century, the results presented here certainly appear as a surprise. The roots of this puzzle have been discussed by Lahoz and Graham (1981) in connection with the more general '$\mu_0 H$ or B' problem; however an open question remains: what happens to the energy flux and accompanying electromagnetic momentum at the boundary of a dielectric permanent magnet? The orthodox viewpoint is discussed by Landau and Lifshitz (1960, p 253). They say that the $\boldsymbol{S} = \boldsymbol{E} \times \boldsymbol{H}$ expression for the flux of energy density follows 'from the condition that the normal component of $\boldsymbol{S}$ is continuous at the boundary'. Since, as a matter of fact, the correct expression for the

electromagnetic momentum density is now $\boldsymbol{g} = \varepsilon_0 \boldsymbol{E} \times \boldsymbol{B}$ and, from Planck's principle, $\boldsymbol{S} = \mu_0^{-1} \boldsymbol{E} \times \boldsymbol{B} = \boldsymbol{E} \times \boldsymbol{H} + \boldsymbol{E} \times \boldsymbol{M}$, the Landau–Lifshitz condition is violated in the case of a dielectric permanent magnet (of sufficient length to set $H \simeq 0$ at the lateral boundaries). If, within the magnet, there is an $\boldsymbol{E}$ field tangential to the boundary, the discontinuity of the normal components of $\boldsymbol{g}$ and $\boldsymbol{S}$ become $\Delta g_n = (1/c^2)|\boldsymbol{E} \times \boldsymbol{M}|$ and $\Delta S_n = |\boldsymbol{E} \times \boldsymbol{M}|$. This is not a paradox in the Livens (updated) theory since during the time interval δt, while the $\boldsymbol{E}$ field is uniformly (say) introduced, a uniform force density $f = \mu_0 \boldsymbol{M} \times \nabla \times \boldsymbol{H}$ $(= (1/c^2) \boldsymbol{M} \times \dot{\boldsymbol{E}})$ is acting on the magnet, fulfilling $\delta g_n = |\int_0^{\delta t} f \, \mathrm{d}t|$, whereas outside the magnet $\delta g_n = g_n = 0$. Thus the isolated block of pure electromagnetic momentum confined within the magnet boundaries, originating at $t = \delta t$ and carried by the vacuum, is the opposite of the momentum given to the magnet (at $t = \delta t$) by that impulsive force (which, mistakenly, is not recognised or included in the total phenomenological force density of the orthodox theory).

Similarly the gained kinetic energy of the magnet would represent, initially at least, an energy flux density moving (with negligible velocity) in the opposite direction to $\boldsymbol{E} \times \boldsymbol{M}$. Although it would seem to follow that the vacuum (to which $\boldsymbol{E} \times \boldsymbol{M}$ is attached) acts as a reservoir of infinite inertia (Lorentz's hypothesis of an aether at rest), such a concept is not inconsistent with any fundamental law.

Acknowledgments

The mechanical elaboration of the (Ni–Zn)- and Ba-ferrite samples for this experiment, the lengthy and involved mechanical work leading to sintered magnetite samples used in the preliminary experiment and several precision pieces of the apparatus are credited to Mr D E Britton. The preparation of the natural magnetite sample and suspension along with other precision work are credited to Mr R J Carder. We are also indebted to Mr J Friel for the elaboration of a first ferrite sample and the manufacture of a preliminary stainless-steel dewar which decisively helped in assessing the possibilities for a practical realisation of the final experiment as reported here. Important contributions of welding and lathe work are credited to Mr A W Ffrench. The innovative character of this five-year task has required the collaboration of several workshops and many members of the technical staff to whom we have to credit for their specialised contributions and patient understanding.

The Natural Sciences and Engineering Research Council of Canada has financially supported this experiment.

References

Calhoun B A 1954 *Phys. Rev.* **94** 1577
Domenicali C A 1950 *Phys. Rev.* **78** 458
Einstein A and Laub J 1908 *Ann. Phys., Lpz* **26** 541
Flanders P J and Shtrikman S 1962 *J. Appl. Phys.* **33** Suppl no 3 1318
Graham G M and Lahoz D G 1980 *Nature* **285** 154
—— 1981 *J. Phys. A: Math. Gen.* submitted for publication
Jacobs I S 1959 *J. Phys. Chem. Solids* **11** 1
Lahoz D G and Graham G M 1979a *Can. J. Phys.* **57** 667
—— 1979b *Phys. Rev. Lett.* **42** 1137
—— 1981 *Can. J. Phys.* **59** 1

Landau L D and Lifshitz E M 1960 *Electrodynamics of Continuous Media* (New York: Pergamon)
Livens G H 1918 *The Theory of Electricity* (Cambridge: University Press)
Novak M M 1980 *Fortschr. Phys.* **28** 285
Page L and Adams N I 1940 *Electrodynamics* (New York: Van Nostrand)
Pauthenet R 1952 *Ann. Physique* **7** 710
Penfield P and Haus H A 1967 *Electrodynamics of Moving Media* (Cambridge, MA: MIT Press)
Richter H G and Dietrich H E 1968 *IEEE Trans. Mag.* **4** 263
Smit J and Wijn H P J 1960 *Ferrites* (New York: Wiley)
Stuijts A L *et al* 1964 *IEEE Trans. Comm. Elect.* **83** 728